Approximation of internodal conductivities in numerical simulation of one-dimensional infiltration, drainage, and capillary rise in unsaturated soils

Adam Szymkiewicz[1]

Received 15 December 2008; revised 15 June 2009; accepted 1 July 2009; published 1 October 2009.

[1] When the unsaturated flow equation is solved with the finite difference method, the water flux between two adjacent nodes of the grid is approximated with a discrete form of Darcy's law. It requires the average value of the hydraulic conductivity in the considered grid block. Since the hydraulic conductivity in unsaturated soil is a highly nonlinear function of the water potential, the nodal conductivities can vary by multiple orders of magnitude, which makes the choice of the appropriate averaging procedure a nontrivial task. In this paper we present a new method to calculate the internodal conductivity for an arbitrary type of the conductivity function and arbitrary large grid size. It is based on the analysis of approximate profiles of the water potential head for steady flow between nodes. Numerical experiments show that the method is reasonably accurate for a wide range of soil types, for both steady and unsteady flow simulations.

Citation: Szymkiewicz, A. (2009), Approximation of internodal conductivities in numerical simulation of one-dimensional infiltration, drainage, and capillary rise in unsaturated soils, *Water Resour. Res.*, *45*, W10403, doi:10.1029/2008WR007654.

1. Introduction

[2] Many applications of civil and environmental engineering require numerical simulation of the water flow in the unsaturated zone of soil. The unsaturated flow is commonly described with the Richards' equation (RE), based on the assumption that the air phase in soil is at constant atmospheric pressure. Numerical solution of RE is not trivial, due to nonlinear relations between the soil water potential head, volumetric water content, and hydraulic conductivity. This paper focuses on the problems caused by the nonlinear dependence of the hydraulic conductivity on the water potential head, occurring in the finite difference solution of one-dimensional RE. Since the values of the hydraulic conductivity at two adjacent nodes can vary by several orders of magnitude, some kind of average conductivity should be used in order to approximate the water flux between nodes with a finite difference formula. The most popular approach seems to be the standard arithmetic mean of the nodal values; however, it can produce significant errors in some situations [e.g., *Haverkamp and Vauclin*, 1979; *Baker et al.*, 1999; *Belfort and Lehmann*, 2005]. Alternative propositions include, among others, the geometric, upstream-weighted, and integrated means. Comparisons of various approximations can be found in the literature [e.g., *Haverkamp and Vauclin*, 1979; *Srivastava and Guzman-Guzman*, 1995; *Miller et al.*, 1998; *Belfort and Lehmann*, 2005], but the conclusions are difficult to generalize, since in each case numerical simulations were performed for a limited number of soil materials and grid sizes.

[3] A consistent framework for the assessment of various averaging schemes is provided by the so-called Darcian mean approach [*Warrick*, 1991]. In this method the average internodal conductivity is calculated from the Darcy's law assuming steady state flow between two adjacent nodes, which leads to very accurate results. This concept was further developed by *Baker* [1995, 2000], *Baker et al.* [1999], and *Gastó et al.* [2002], who approximated the Darcian means either as a weighted average of the integrated mean and the conductivity of the upper node or as a weighted average of the two nodal conductivities. The formula of *Gastó et al.* [2002] is simple to implement, but it can be applied neither for an arbitrary type of the conductivity function nor for arbitrary large spatial steps. The method of *Baker* [2000] does not have these limitations, but it is relatively complex in implementation. In this paper we propose a scheme which can be applied to any type of the conductivity function and requires only a little more numerical effort than the integrated mean approach.

2. Background

[4] The one-dimensional (1-D) form of RE can be written as follows [e.g., *Kutílek and Nielsen*, 1994; *Warrick*, 2003]:

$$\frac{\partial \theta(h)}{\partial t} + \frac{\partial q}{\partial z} = 0 \tag{1a}$$

$$q = -K(h)\left(\frac{\partial h}{\partial z} - \gamma\right), \tag{1b}$$

where h is the soil water potential head (negative in the unsaturated zone), $\theta(h)$ is the volumetric water content, q is the volumetric water flux, $K(h)$ is the hydraulic conductivity, and γ is the cosine of the angle between the z axis and

[1]Faculty of Civil and Environmental Engineering, Gdańsk University of Technology, Gdańsk, Poland.

0043-1397/09/2008WR007654

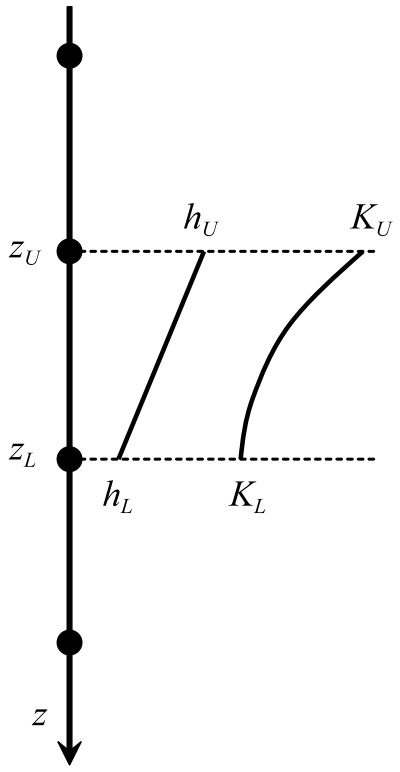

Figure 1. Spatial discretization of one-dimensional unsaturated flow equation with the finite difference method.

the direction of the gravity force. For vertical flow $\gamma = 1$ and for horizontal flow $\gamma = 0$, while for flow in an inclined column γ assumes intermediate values. If mass forces other than gravity are present (e.g., during flow in a centrifuge), γ may assume values larger than one [e.g., *Caputo and Nimmo*, 2005]. Equations (1a) and (1b) should be complemented by specifying the hydraulic functions, relating θ, h, and K [e.g., *Brooks and Corey*, 1964; *Mualem*, 1976; *van Genuchten*, 1980].

[5] In order to solve equations (1a) and (1b) numerically, the finite difference method is often used. The solution domain is discretized with a number of nodes (Figure 1), and the water fluxes between adjacent nodes are approximated according to the following formula:

$$q_{UL} = -K_{AV}\left(\frac{h_L - h_U}{z_L - z_U} - \gamma\right) = -K_{AV}\left(\frac{\Delta h}{\Delta z} - \gamma\right), \quad (2)$$

where the indices U and L refer to the upper and the lower nodes, respectively, and K_{AV} is the average internodal conductivity. This spatial discretization scheme can be combined with a number of approaches for the discretization in time, ranging from the relatively simple (and most common) first-order fully implicit Euler scheme [e.g., *Celia et al.*, 1990; *Šimůnek et al.*, 1998] to the sophisticated high-order backward difference formulae [e.g., *Miller et al.*, 1998]. Regardless of the method used for the discretization in time, the overall accuracy of the numerical scheme depends very much on the spatial discretization error, which in turn is mostly determined by the method of estimating K_{AV}. A similar problem arises when the finite element method is used for spatial discretization of RE. In such a case, the average conductivity over a single element has to be estimated. Some of the most popular choices for K_{AV} include

Arithmetic mean [e.g., *Celia et al.*, 1990; *van Dam and Feddes*, 2000]

$$K_{ARIT} = 0.5\,(K_U + K_L) \quad (3a)$$

Geometric mean [e.g., *Haverkamp and Vauclin*, 1979]

$$K_{GEOM} = \sqrt{K_U K_L} \quad (3b)$$

Upstream-weighted mean [e.g., *Forsyth et al.*, 1995; *Oldenburg and Pruess*, 1993]

$$K_{UPS} = \begin{cases} K_U, & \text{if} \quad \dfrac{\Delta h}{\Delta z} - \gamma \le 0 \\ K_L, & \text{if} \quad \dfrac{\Delta h}{\Delta z} - \gamma > 0 \end{cases} \quad (3c)$$

Integrated mean [e.g., *Srivastava and Guzman-Guzman*, 1995; *Miller et al.*, 1998]

$$K_{INT} = \begin{cases} \dfrac{1}{(h_L - h_U)}\displaystyle\int_{h_U}^{h_L} K(\psi)d\psi = \dfrac{\Phi(h_L) - \Phi(h_U)}{(h_L - h_U)}, & \text{if} \quad h_U \neq h_L \\ K_U, & \text{if} \quad h_U = h_L \end{cases}, \quad (3d)$$

where $\Phi(h)$ denotes the Kirchhoff transformed variable,

$$\Phi(h) = \int_{-\infty}^{h} K(\psi)d\psi.$$

Other, less often used averaging schemes include harmonic mean [*Oldenburg and Pruess*, 1993; *Manzini and Ferraris*, 2004], computing conductivity from the arithmetic average of nodal saturations [*Miller et al.*, 1998] or nodal potential heads [*Haverkamp and Vauclin*, 1979], or numerical approximations to K_{INT} based on low-order quadratures [*Srivastava and Guzman-Guzman*, 1995]. Previous research has shown that none of the averaging schemes listed above produces satisfactory results in the whole range of grid sizes, soil textures, and flow directions. Most of the studies reported up till now focused on vertical infiltration into dry soil, and showed that inaccurate estimation of K_{AV} may lead to considerable overestimation or underestimation of the position of the wetting front [*Haverkamp and Vauclin*, 1979; *Warrick*, 1991; *Belfort and Lehmann*, 2005]. Moreover, for large Δz the underestimation of K_{AV} produce oscillatory solutions, inadmissible from the physical point of view [*Baker et al.*, 1999; *Szymkiewicz*, 2007].

[6] It is known that the value of K_{AV} depends on the ratio of capillary to gravity forces at the scale of a single grid block [*Warrick*, 1991; *Zaidel and Russo*, 1992; *Baker*, 2000]. The integrated mean K_{INT} is an accurate approximation of K_{AV} for capillary-dominated flow, either horizontal ($\gamma = 0$) or vertical with $|\Delta h/\Delta z| \gg \gamma$ [e.g., *Miller et al.*, 1998; *Belfort and Lehmann*, 2005]. On the other hand, for gravity-dominated infiltration (large Δz) good results are obtained with the upstream-weighted mean K_{UPS} [*Forsyth et al.*, 1995; *Baker et al.*, 1999]. Upstream weighting is also

the preferred choice for advection-dominated two-phase flow [*Helmig and Huber*, 1996]. This observation motivated some authors [e.g., *Zaidel and Russo*, 1992] to split the total water flux in two parts: a diffusive one (capillarity-related) and an advective one (gravity-related) and to use different approximations of the internodal conductivity for each component:

$$q_{UL} = -K_{CAP}\frac{h_L - h_U}{\Delta z} + K_{GRAV}\,\gamma, \tag{4}$$

where K_{CAP} and K_{GRAV} correspond to the capillary-driven and gravity-driven part of the total flux, respectively. *Zaidel and Russo* [1992] used the standard arithmetic mean K_{ARIT} for K_{GRAV}. For K_{CAP} they developed an asymptotic weighted approximation, which can be used for soils described by van Genuchten–Mualem hydraulic functions. *Zhang and Ewen* [2000] used a similar scheme with K_{INT} for K_{CAP} and K_{ARIT} or K_{UPS} for K_{GRAV}. If the capillary and gravity forces act in the opposite directions, care should be taken that q has the sign consistent with the sign of the total hydraulic gradient ($\Delta h/\Delta z - \gamma$). Otherwise, nonphysical inverse fluxes may occur for some combinations of K_{CAP} and K_{GRAV}. To avoid this problem, *Ross* [2003] recommended using a weighted arithmetic mean for K_{GRAV}, with adjustable weighting coefficients.

[7] Accurate estimation of K_{AV} is possible using the concept of Darcian means introduced by *Warrick* [1991]. When solving an unsteady flow problem, the internodal conductivity K_{AV} for any pair of nodes should be chosen in such a manner that the water flux obtained with equation (2) is equal to the water flux for the steady state flow between the two nodes. The steady flow is described by the following equation:

$$-\frac{\partial}{\partial z}\left(K(h)\left(\frac{\partial h}{\partial z} - \gamma\right)\right) = 0, \quad z_U \le z \le z_L \tag{5a}$$

with the boundary conditions

$$h(z_U) = h_U \tag{5b}$$

$$h(z_L) = h_L. \tag{5c}$$

[8] Depending on the complexity of the $K(h)$ function, the steady state problem given by equations (5a) and (5b) can be solved either analytically [*Baker*, 1995] or numerically [*Warrick*, 1991; *Baker*, 2000; *Gastó et al.*, 2002], yielding the fine-scale pressure distribution $h(z)$ between the two nodes z_U and z_L and the corresponding value of q_{STEADY}, which is constant within the interval. The Darcian conductivity is then computed as

$$K_{DAR} = \frac{-q_{STEADY}}{((h_L - h_U)/\Delta z - \gamma)}. \tag{6}$$

It is impossible to use this approach directly for practical purposes, as the numerical solution of the steady state flow equation for each pair of nodes is a problem in itself and would excessively lengthen the time of computations for the unsteady problem. Thus *Warrick* [1991] and later *Gastó et al.* [2002] proposed expressing the internodal conductivity as a weighted arithmetic mean of the nodal values:

$$K_{GASTO} = wK_U + (1 - w)K_L, \tag{7}$$

where the weighting coefficient $w \in \langle 0;1\rangle$ is chosen in such a way that $K_{AV} \approx K_{DAR}$. *Gastó et al.* [2002] found w to be a function of four variables: K_U, K_L, $\Delta z/h_g$, and n, where h_g and n are soil-dependent parameters appearing in Brooks-Corey and van Genuchten–Mualem conductivity functions. Additionally, the function w contains five fitting parameters obtained by a numerical calibration procedure. While accurate and useful in many situations, the approach of *Gastó et al.* [2002] has some limitations. First, the fitting parameters are provided only for the standard functions of Brooks-Corey and van Genuchten–Mualem (with connectivity parameter equal to 0.5). For any other type of function a separate calibration procedure would be necessary, which involves a considerable numerical effort. Second, the method cannot be used for $\Delta z \gg h_g$ because the empirical formula may produce negative values of w and K_{GASTO} [see *Gastó et al.*, 2002, equations (8a), (9), (10)]. This may be inconvenient for coarse textured soils, characterized by small values of h_g (of the order of a few centimeters).

[9] Another type of Darcian averaging scheme was developed by *Baker* [1995], *Baker et al.* [1999], and *Baker* [2000]. The internodal conductivity is written as

$$K_{BAKER} = (1 - w_v)K_{INT} + w_vK_U, \tag{8}$$

where w_v is a weighting coefficient from the range $\langle 0,1\rangle$. In contrast to equation (7), equation (8) defines the internodal conductivity as a linear combination of its actual limit values. The weighting coefficient w_v is given by a relatively complex analytical formula and requires that the conductivity function $K(h)$ be inverted to compute an intermediate value of the water potential head corresponding to the geometric mean of the nodal conductivities, $h(K = \sqrt{K_UK_L})$. Some of the conductivity functions (including the widely used van Genuchten–Mualem function) cannot be inverted analytically, and thus additional numerical effort is required to compute K_{AV}.

[10] One should note that even if a simple conductivity averaging scheme is used, the error related to incorrect approximation of the fluxes can be significantly reduced by grid refinement in the zones where large gradients of water potential are expected. In typical hydrological simulations, improvement can be obtained by local grid refinement near the soil surface [e.g., *van Dam and Feddes*, 2000]. More sophisticated adaptive schemes have been also developed, where the grid is dynamically refined during the solution, according to the formal estimation of the spatial discretization error [*Miller et al.*, 2006]. Despite the utility of these methods, it seems that there still is interest in developing conductivity averaging schemes yielding accurate results for a wide range of Δz values and $K(h)$ functions, which can be relatively easily implemented into existing numerical codes, often based on low-order spatial and temporal approximations [e.g., *Šimůnek et al.*, 1998; *Belfort and Lehmann*, 2005; *Pei et al.*, 2006]. On the other hand, if more accurate conductivity averaging schemes were used in conjunction with spatially adaptive approaches, one could expect an

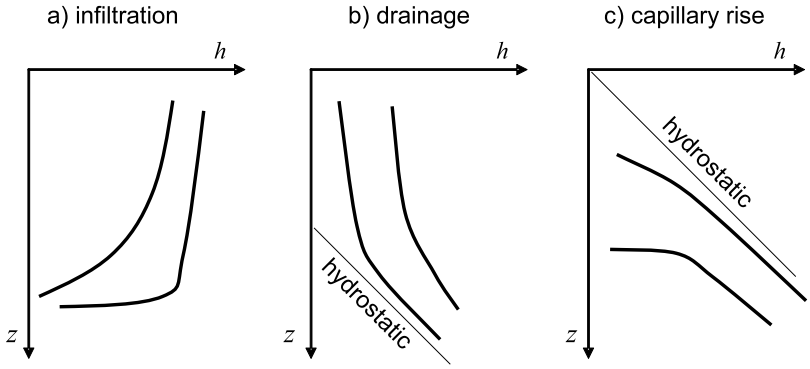

Figure 2. Approximate forms of the steady state water potential head profiles for different types of flow [after *Warrick and Yeh*, 1991].

increase in their efficiency, since the required accuracy would be achieved with a lower level of grid refinement.

3. Approximation of the Internodal Conductivity for Various Types of Flow

3.1. Limit Values of the Internodal Conductivity

[11] The results reported by *Warrick* [1991], *Baker* [2000, 2006], and *Gastó et al.* [2002] suggest that the most accurate approximation of K_{AV} is given by the Darcian mean, corresponding to the steady flow between two nodes. Thus the method developed here is based on the analysis of steady state distribution of the potential head, $h(z)$, between z_U and z_L. The shape of the potential profile depends on the type of flow. Three major cases can be distinguished [*Warrick and Yeh*, 1991]: $\Delta h/\Delta z < 0$ (Figure 2a), $\gamma > \Delta h/\Delta z > 0$ (Figure 2b), and $\Delta h/\Delta z > \gamma$ (Figure 2c).

[12] The first case corresponds to infiltration in dry soil. The second case describes either drainage or infiltration toward a nearby water table. The third case represents vertical uptake of water by capillary forces. For simplicity these types of flow will be called infiltration, drainage, and capillary rise, respectively. For each type of flow the capillary gradient $\Delta h/\Delta z$ varies in a specific range. Previous research [*Baker et al.*, 1999; *Baker*, 2000, 2006] allows us to determine the values of K_{AV} corresponding to the limit values of $\Delta h/\Delta z$:

Infiltration

$$K_{AV} \to K_{INT} \quad \text{for} \quad \frac{\Delta h}{\Delta z} \to -\infty \quad \text{and} \quad K_{AV} \to K_U \quad \text{for} \quad \frac{\Delta h}{\Delta z} \to 0$$

Drainage

$$K_{AV} \to K_U \quad \text{for} \quad \frac{\Delta h}{\Delta z} \to 0 \quad \text{as well as for} \quad \frac{\Delta h}{\Delta z} \to \gamma$$

Capillary rise

$$K_{AV} \to K_U \quad \text{for} \quad \frac{\Delta h}{\Delta z} \to \gamma \quad \text{and} \quad K_{AV} \to K_{INT} \quad \text{for} \quad \frac{\Delta h}{\Delta z} \to \infty.$$

[13] The above relations and the difference in shapes of the potential head profiles shown in Figure 2 suggest that a different approximating formula is needed for each of the three types of flow. Note that two other cases are possible, when $\Delta h = 0$ and $\Delta h/\Delta z = \gamma$, respectively. In each of these cases $K_{AV} = K_U$.

3.2. Infiltration

[14] The internodal conductivity for infiltration should vary between K_{INT} and K_U, depending on the ratio of the capillary and gravity forces at the grid block scale. For a gravity-dominated flow, oscillations may arise in the numerical solution if the applied averaging method underestimates K_{AV} with respect to the Darcian mean. This effect can be explained by the example of a simple numerical grid shown in Figure 3a. The grid is composed of three nodes, z_0, z_U, and z_L. Let us denote the fluxes in the upper and lower part of the domain by $q^{(1)}$ and $q^{(2)}$, respectively, and the corresponding internodal conductivities by $K_{AV}^{(1)}$ and $K_{AV}^{(2)}$. For steady flow the physically admissible solutions are shown by solid lines. They are obtained when the value of the potential h_U at the intermediate note z_U is between $h_A = (h_L + h_0)/2$ and h_0. The value of h_U should be such that the flux at point z_U is continuous. The case of $h_U = h_A$ corresponds to the saturated flow with $K_{AV}^{(1)} = K_{AV}^{(2)}$ and uniform hydraulic gradient in the domain. For unsaturated flow $K_{AV}^{(1)} > K_{AV}^{(2)}$ and with $h_U = h_A$, one has $q^{(1)} > q^{(2)}$, and thus h_U should be greater than h_A. In the limit one can arrive at $h_U = h_0$, and consequently $q^{(1)} = K_U$. If the applied method of averaging underestimates $K_{AV}^{(2)}$, it may happen that even in such a case one has still $q^{(1)} > q^{(2)}$. In order to equilibrate the two fluxes, h_U would then assume values larger than h_0, producing oscillations in the numerical solution (indicated by the dashed line in Figure 3a). Obviously, the maximum possible amplitude of the oscillations will not exceed Δz, since for $h_U = h_0 + \Delta z$ one obtains the hydrostatic potential distribution between z_0 and z_U, and thus $q^{(1)} = 0 < q^{(2)}$. A similar analysis based on three-point grid was carried out by *Baker* [2006] to show deficiencies of many commonly used averaging methods. In the present paper it is further developed to derive a more accurate approximation of the internodal conductivity. It should be noted that oscillation-free solution is ensured when $K_{AV}^{(2)}$ is approximated in such a manner that $q^{(2)} \geq q^{(1)}$ for $h_U = h_0$, which can be written as

$$\gamma K_U \leq -K_{AV}^{(2)} \left(\frac{h_L - h_U}{\Delta z} - \gamma \right) \tag{9}$$

$$K_{AV}^{(2)} \geq \frac{\gamma K_U}{\gamma - \Delta h/\Delta z}, \tag{10}$$

where $\Delta h = h_L - h_U < 0$. Equation (10) represents a sufficient, although not necessary condition for a non-

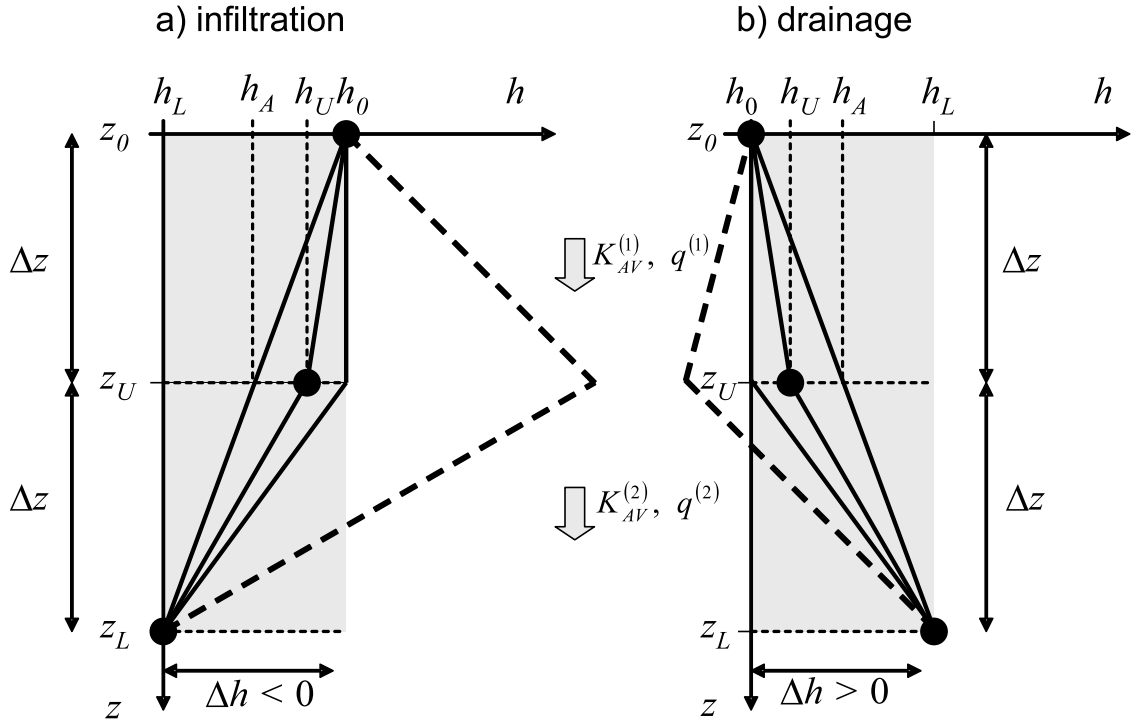

Figure 3. Approximate profiles of the water potential head in the numerical solution of steady (a) infiltration and (b) drainage, for $\gamma = 1$ Solid lines represent physically admissible profiles, and dashed lines represent physically inadmissible oscillatory profiles resulting from underestimation (Figure 3a) or overestimation (Figure 3b) of the internodal conductivity between nodes z_U and z_L.

oscillating solution. In some situations physically admissible profiles can be obtained for smaller values of $K_{AV}^{(2)}$, but the use of the presented approximation guarantees an oscillation-free solution for all cases. Note that previously some authors recommended using the upstream-weighted mean K_{UPS} to eliminate oscillations for gravity-driven infiltration [*Forsyth et al.*, 1995] or for advection-dominated two-phase flow [*Helmig and Huber*, 1996]. For downward infiltration $K_{UPS} = K_U$, and thus the inequality (10) is satisfied, but the value of the interblock conductivity can be significantly overestimated. The right-hand side of equation (10) represents the minimum value of $K_{AV}^{(2)}$, which ensures oscillation-free solution and gives a more accurate estimation of $K_{AV}^{(2)}$.

[15] As $\Delta h/\Delta z \to -\infty$, the limit value of $K_{AV}{}^{(2)}$ given by equation (10) tends to 0. In such a case, however, we can use the integrated mean K_{INT} to estimate K_{AV}. The general formula for approximating K_{AV} between two adjacent nodes z_U and z_L has thus the following form:

$$K_{AV} = \max\left(K_{INT}, \frac{\gamma K_U}{\gamma - (h_L - h_U)/\Delta z}\right), \tag{11}$$

which allows us to obtain the correct limit values of K_{AV} for $\Delta h/\Delta z \to -\infty$ and $\Delta h/\Delta z \to 0$. Note that the analysis presented remains valid for a nonuniform nodal spacing. In such a case the value of Δz in equation (11) will simply be different for each pair of nodes.

3.3. Drainage

[16] A similar estimation for K_{AV} as given by equation (10) can be derived for the case of drainage flow. Consider the numerical grid shown in Figure 3b. Physically admissible water potential profiles correspond to the range of $h_U \in \langle h_0, h_A\rangle$, where $h_A = (h_0 + h_L)/2$. In unsaturated conditions $K_{AV}^{(1)}$ is smaller than $K_{AV}^{(2)}$. Thus the hydraulic gradient in the lower part of the domain should be smaller. In the limit case, when $h_U = h_0$, the average conductivity between nodes z_U and z_L should fulfill the following condition:

$$\gamma K_U \geq -K_{AV}^{(2)}\left(\frac{h_L - h_U}{\Delta z} - \gamma\right), \tag{12}$$

which implies

$$K_{AV}^{(2)} \leq \frac{\gamma K_U}{\gamma - \Delta h/\Delta z}. \tag{13}$$

If $K_{AV}^{(2)}$ is overestimated and does not satisfy equation (13), the water fluxes $q^{(1)}$ and $q^{(2)}$ equilibrate for $h_U < h_0$ (the minimum possible value being $h_U = h_L - \Delta z$, which gives $q^{(2)} = 0$). As in the previous case, equation (13) represents a sufficient, but not necessary condition to obtain oscillation-free solution.

[17] Note that as $\Delta h/\Delta z$ approaches γ, the limit value of $K_{AV}^{(2)}$ provided by equation (13) tends to infinity. For such a case another estimation is required. To this order let us consider an approximate water potential head profile within a single grid block between z_U and z_L, assuming that Δz is larger than Δh only by a small value δz, i.e., the hydrostatic distribution of the water potential is approached (Figure 4). We introduce an intermediate point z_R, which divides the grid block in two unequal intervals $\langle z_U, z_R\rangle$ and $\langle z_R, z_L\rangle$. For

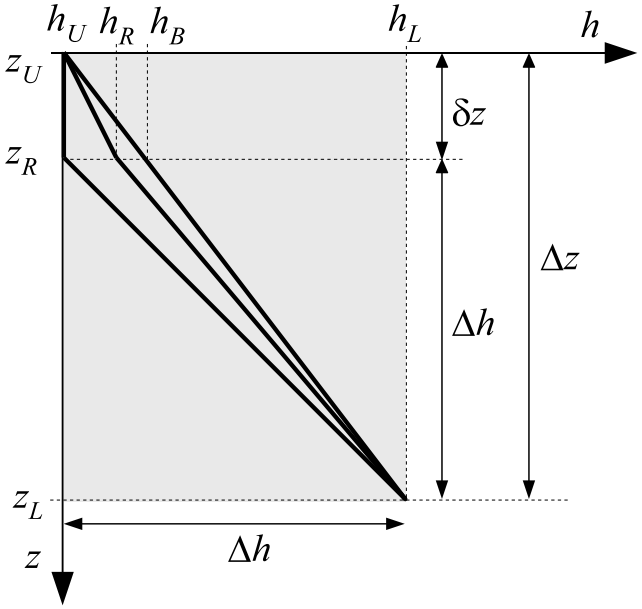

Figure 4. Approximate steady state profile of the water potential head within a single grid block during drainage when $\Delta h/\Delta z$ approaches $\gamma = 1$.

linear potential distribution the value of h_R would be equal to $h_B = (h_L - (\Delta h)^2/(\gamma \Delta z))$. In unsaturated conditions the potential head h_R should be between h_U and $h_B = (h_L - (\Delta h)^2/(\gamma \Delta z))$. From Figure 4 we may assume that the hydraulic gradient within the segment $\langle z_R, z_L \rangle$ is approximately the same as the hydraulic gradient between z_U and z_L, and both of them are close to zero, $[(h_L - h_R)/(z_L - z_R) - \gamma] \approx [(h_L - h_U)/(z_L - z_U) - \gamma] \rightarrow 0$. On the other hand, for the conditions close to the hydrostatic state the value of the internodal conductivity approaches the conductivity of the upper node. Thus the average conductivity in the segment $\langle z_R, z_L \rangle$ is approximately $K(h_R) = K_R$. The value of K_R is not known; it lies between K_U and K_B. Let us assume $K_R \approx K_B$ (if one assumed K_R equal to K_U, then the conductivity for the whole grid block would be equal K_U, which is correct only for the limit case when $\Delta h/\Delta z = \gamma$). Consequently the water flux between z_R and z_L is estimated as

$$q^{(2)} \approx -K_R\left(\frac{h_L - h_R}{\Delta z - \delta z} - \gamma\right) \approx -K_B\left(\frac{h_L - h_U}{\Delta z} - \gamma\right). \quad (14)$$

For steady flow the flux $q^{(2)}$ should be equal to the average flux in the domain $q_{UL} = -K_{AV}\,[(h_L - h_U)/\Delta z - \gamma]$, which implies

$$K_{AV} = \frac{-q^{(2)}}{(h_L - h_U)/\Delta z - \gamma} \approx K_B = K\left(h_L - (\Delta h)^2/(\gamma\,\Delta z)\right). \quad (15)$$

For $\Delta h \rightarrow \Delta z$, equation (15) gives the expected limit value $K_{AV} \rightarrow K_U$, while for $\Delta h \ll \Delta z$ equation (15) gives $K_{AV} \rightarrow K(h_L) = K_L$ (which is an overestimation). In order to estimate K_{AV} with a reasonable accuracy for an arbitrary value of $\Delta h/\Delta z$ from the range (0; γ) it is suggested to take the smaller value of the two estimations given by equations (13) and (15):

$$K_{AV} = \min\left(\frac{\gamma\,K_U}{\gamma - \Delta h/\Delta z},\ K\left(h_L - (\Delta h)^2/(\gamma \Delta z)\right)\right). \quad (16)$$

3.4. Capillary Rise

[18] The physically admissible steady state profiles for capillary rise are shown in Figure 5. In this case an error in the estimated value of K_{AV} does not produce oscillations. Actually, the difference between the smaller conductivity in the upper part and the larger conductivity in the lower part of the domain can be always compensated for by the fact that the hydraulic gradient in the lower part can be set arbitrarily close to zero (hydrostatic state), thus enabling us to equilibrate fluxes. Consequently, no limit values for K_{AV} similar to the ones given by equation (10) or (13) can be derived. However, one can still use the approximate shape of the steady state pressure profile to derive a reasonably accurate estimation for K_{AV}. Consider the situation shown in Figure 5. The interval (z_U, z_L) is divided by the point z_R, located at some small distance δz below z_U. We assume that

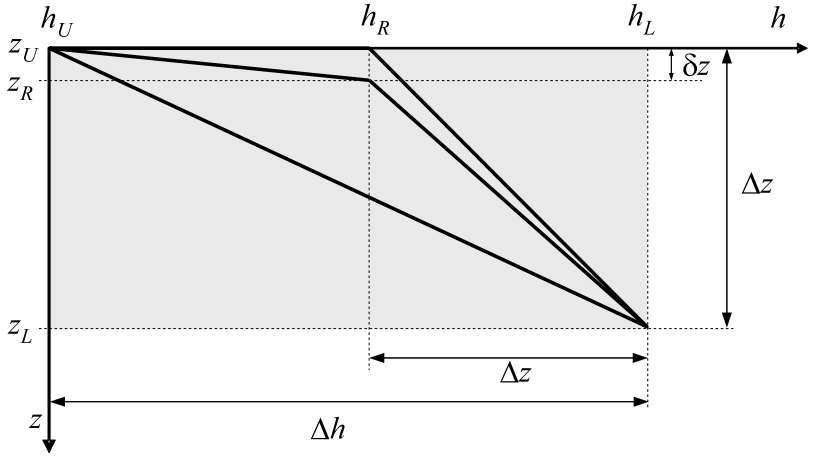

Figure 5. Approximate steady state profile of the water potential head within a single grid block during capillary rise ($\gamma = 1$).

Table 1. Hydraulic Parameters of the Soils Used for Accuracy Evaluation

Soil	Equations for $K_{REL}(h)$	h_g (cm) (or A [ ])	n [ ] (or λ [ ])	m	η [ ]	L [ ]
1	(20a), (20b)	6.9	2.680	0.627	...	0.50
2	(20a), (20b)	13.3	1.890	0.471	...	0.50
3	(20a), (20b)	50.0	1.410	0.291	...	0.50
4	(20a), (20b)	200.0	1.090	0.083	...	0.50
5	(21a), (21b)	7.2	0.592	...	5.88	...
6	(21a), (21b)	14.7	0.322	...	8.71	...
7	(21a), (21b)	20.7	0.211	...	11.98	...
8	(21a), (21b)	34.2	0.127	...	18.25	...
9	(20a), (20b)	38.5	2.230	0.552	...	−1.28
10	(20a), (20b)	24.5	1.190	0.160	...	−6.97
11	(20a), (21b)	30.2	7.000	0.710	7.00	...
12	(20a), (21b)	6.2	2.970	0.327	5.05	...
13	(22)	1.175×10^6	4.740	...	...	...
14	(23)	1.0	...	...	...	...
15	(23)	100.0	...	...	...	...

the lower part of the profile is close to the hydrostatic state, which implies $K_{AV}^{(2)} = K(h_R)$. For the upper part of the profile we assume that $h_R - h_U \gg \gamma(z_R - z_U)$, implying capillary-dominated flow and consequently $K_{AV}^{(1)} = K_{INT}^{(1)} = \int_{h_U}^{h_R} K(\psi)d\psi/(h_R - h_U)$. The average internodal conductivity will be equal to the weighted harmonic mean of $K_{AV}^{(1)}$ and $K_{AV}^{(2)}$:

$$K_{AV} = \frac{\Delta z K_{AV}^{(1)} K_{AV}^{(2)}}{(\Delta z - \delta z)K_{AV}^{(1)} + \delta z K_{AV}^{(2)}}. \tag{17}$$

The value of δz can be obtained from the flux continuity condition at node z_R:

$$-K_{AV}^{(1)}\left(\frac{\Delta h - \gamma\,\Delta z}{\delta z} - \gamma\right) = -K_{AV}^{(2)}\left(\frac{\gamma \Delta z}{\Delta z - \delta z} - \gamma\right). \tag{18}$$

Equation (18) represents a quadratic equation for δz, with one positive and one negative root. The positive root is

$$\delta z = \frac{-\Delta h + \sqrt{(\Delta h)^2 + 4\left(K_{AV}^{(2)}/K_{AV}^{(1)} - 1\right)\gamma\,(\Delta h - \gamma\,\Delta z)\Delta z}}{2\,\gamma\left(K_{AV}^{(2)}/K_{AV}^{(1)} - 1\right)}. \tag{19}$$

Substituting equation (19) into (17) one obtains the final estimation for K_{AV}.

3.5. Summary

[19] The proposed method for calculating the internodal conductivity can be summarized in form of the following pseudocode:

```
define function FK(h)
// hydraulic conductivity as function of the water potential
   head
define function FKintegrated(h1,h2)
// integrated mean conductivity
input hU, hL, zU, zL, Gamma
Dh = hL−hU, Dz = zL−zU, KU = FK(hU), KL = FK(hL)
if (Dh = = 0.0) or (Dh = = Gamma*Dz) then
// uniform or hydrostatic h distribution
KAV = KU
else if (Dh/Dz < 0) then
// infiltration
K1 = FKintegrated(hU,hL)
K2 = Gamma*KU/(Gamma−Dh/Dz)
KAV = max(K1,K2)
else if (Dh/DZ < Gamma)
// drainage
K1 = Gamma*KU/(Gamma−Dh/Dz)
K2 = FK(hL−Dh*Dh/(Gamma*Dz))
KAV = min(K1,K2)
else
// capillary rise
K1 = FKintegrated (hU, hL−Dz)
K2 = FK(hL−Gamma*Dz)
A = sqrt(Dh*Dh+4*(K2/K1−1)*Gamma*(Dh-
   Gamma*Dz)*Dz)−Dh
B = 2*Gamma*(K2/K1−1)
Dz1 = A/B
KAV = Dz*K1*K2/((Dz−Dz1)*K1+Dz1*K2)
end if
```

[20] The algorithm requires two user-defined functions: one for the hydraulic conductivity (FK(h)) and one for the integrated mean conductivity (FKintegrated(h1,h2)). Such a procedure can be easily implemented into existing numerical codes based on finite difference or low-order finite element approximation of the water fluxes.

4. Accuracy Assessment for Steady Flow

[21] The accuracy of the proposed method has been evaluated by comparison with the Darcian mean approach. Darcian means provide the exact values of the internodal conductivity for steady flow and have been shown to be a very good approximation also for transient flow problems [*Warrick*, 1991; *Baker*, 2000; *Gastó et al.*, 2002]. The comparisons were performed for a wide range of soil types, grid sizes, and potential heads.

[22] Fifteen soils were chosen, characterized by a variety of conductivity functions. The conductivity function for each soil is expressed as $K(h) = K_S K_{REL}(h)$, where K_S is the conductivity at saturation and K_{REL} is the dimensionless relative conductivity. K_S is essentially a scaling factor and was assumed equal to unity in each case. The parameters of the $K_{REL}(h)$ functions are listed in Table 1.

[23] Soils 1–4 were taken from the soil database in HYDRUS-1D software [*Šimůnek et al.*, 1998] and correspond to the typical examples of sand, sandy loam, silty loam, and silty clay, as reported by *Carsel and Parrish* [1988]. They are described by the *van Genuchten* [1980] retention function with *Mualem* [1976] conductivity function:

$$S_E = \left(1 + \left|h/h_g\right|^n\right)^{-m}, \tag{20a}$$

$$K_{REL} = S_E^L\left(1 - \left(1 - S_E^{1/m}\right)^m\right)^2, \tag{20b}$$

where S_E is the effective saturation, h_g is a parameter related to the average pore size, n is a parameter related to the pore size distribution, $m = 1 - 1/n$, and L is the connectivity parameter ($L = 0.5$ for Soils 1–4).

[24] The next four soils (5–8) are also taken from Hydrus 1D database and represent the same four textural classes as soils 1–4, but this time characterized by *Brooks and Corey* [1964] hydraulic functions:

$$S_E = |h/h_g|^{-\lambda}, \tag{21a}$$

$$K_{REL} = S_E^{\eta}, \tag{21b}$$

where λ is a parameter depending on soil texture and $\eta = 2.5 + 2/\lambda$. In equations (21a) and (21b) h_g corresponds to the air entry pressure. The equations are valid for $h < h_g$, while for $h \geq h_g$ the medium is fully saturated with $S_E = 1$ and $K_{REL} = 1$.

[25] Soils 9 and 10 correspond to the sand and clay from *Schaap and Leij* [2000], who proposed an improved conductivity function, which is given by equations (20a) and (20b) with the connectivity parameter L assuming negative values.

[26] Soils 11 and 12 are described by the model of *Fuentes et al.* [1992]. It consists of van Genuchten type retention function, equation (20a) with $n = 1 - 2/m$, combined with a Brooks-Corey type conductivity function equation (21b), with an independent parameter η. Soil 11 represents Hostun H38 sand used in the experiments described by *Szymkiewicz et al.* [2008], while soil 12 is the Chernobyl soil from the paper of *Lassabatere et al.* [2006].

[27] Soil 13 is taken from the paper by *Haverkamp et al.* [1977]. It is described by the following conductivity function:

$$K_{REL} = A(A + |h|^n)^{-1}, \tag{22}$$

where A is an empirical parameter.

[28] Finally, soils 14 and 15 are characterized by exponential conductivity function [*Gardner*, 1958], which assumes the following form:

$$K_{REL} = \exp(h/h_g). \tag{23}$$

[29] For each soil the steady state flow equation has been solved for all the possible combinations of h_U, h_L, and Δz from the following sets of values: h_U, h_L = {−1 mm, −1 cm, −10 cm, −1 m, −10 m, − 100 m} and Δz = {1 mm, 1 cm, 2 cm, 10 cm, 20 cm, 50 cm, 1 m, 10 m, 100 m}, excluding the cases when $h_L - h_U = \Delta z$ or when one of the nodal relative conductivities was lower than 10^{-12}. While the values of Δz = 10 m or 100 m seem exceedingly large for any practical purpose, they were included to verify the overall flexibility of the new approximation. For soils described by the Brooks-Corey retention function the value of h_g was subtracted from the values of h_U and h_L, in order to keep unsaturated conditions in the whole domain. In order to ensure high accuracy, numerical solutions of the steady state flow equation were performed on fine grids consisting of up to 6001 nodes. The fluxes between nodes were approximated using the integrated conductivity average K_{INT}; however, for such a fine grid the method of internodal conductivity estimation virtually did not influence the results. The nonlinear system of equations resulting from spatial discretization was solved using the Newton method. In order to ensure convergence we choose the initial approximation of $h(z)$ resembling the expected steady state profile, as shown in Figure 2. The iterative process was stopped when the water fluxes throughout the domain became uniform, i.e., the largest relative difference between fluxes at any two nodes did not exceed 0.1%.

[30] For any single combination of h_U, h_L, and Δz the flux obtained from the solution of the steady flow problem allows us to compute the Darcian mean conductivity K_{DAR} from equation (6), which is considered as the reference value of the internodal conductivity. It can be used to compute the error of any other approximation of K_{AV}, according to the following formula:

$$E = \log \frac{K_{AV}}{K_{DAR}}. \tag{24}$$

The error is expressed in terms of logarithm to facilitate comparisons of the relative errors, which can differ by several orders of magnitude, and to give equal weight to both overestimation and underestimation errors. In order to evaluate the performance of the averaging methods for large sets of results, the following error measures were introduced:

Root mean square error

$$\mathrm{RMSE} = \sqrt{\frac{1}{M}\left(\sum_{i=1}^{M} E_i^2\right)}$$

Maximum observed error (largest overestimation)

$$\mathrm{MAXE} = \max(E_i)_{i=1..M}$$

Minimum observed error (largest underestimation)

$$\mathrm{MINE} = \min(E_i)_{i=1..M},$$

where M is the number of results in the considered set.

[31] The results of the accuracy analysis are presented in Tables 2 and 3. The error measures were computed for the following averaging methods: standard arithmetic mean (K_{ARIT}, equation (3a)), geometric mean (K_{GEOM}, equation (3b)), upstream-weighted mean (K_{UPS}, equation (3c)), integrated mean (K_{INT}, equation (3d)), the method of *Baker* [2000] (K_{BAKER}), the method of *Gastó et al.* [2002] (K_{GASTO}), and the proposed new method (K_{NEW}). Table 2 presents root-mean-square error (RMSE) values obtained with different averaging methods for each of the 15 soils and the average RMSE for the ensemble of soils. Note that K_{GASTO} was computed only for soils 1–8, which are described by the standard Brooks-Corey or Mualem–van Genuchten functions, and only for the cases where $\Delta z \leq h_g$ for the considered soil. K_{BAKER} was computed only for the cases where the function $K(h)$ can be inverted analytically, i.e., for soils 5–8 and 11–15. It can be seen that the methods based on Darcian means, i.e., K_{GASTO}, K_{BAKER}, and K_{NEW} give significantly smaller errors than the other methods. Note that the errors are expressed in terms of logarithm, and thus RMSE = 0.16 corresponds to 45% relative error in the value of K_{AV}, while R_{MSE} = 1.0 corresponds to 1000% relative error in K_{AV}. K_{NEW} gives the lowest average value of RMSE for most of the considered soils (except soils 14 and 15) and the lowest average RMSE for the ensemble of soils. Soils 14 and 15 are

Table 2. RMSE Values for Different Soils Obtained With Various Averaging Methods[a]

Soil	K_{NEW}	K_{BAKER}	K_{GASTO}	K_{ARIT}	K_{GEOM}	K_{UPS}	K_{INT}
1	0.16	...	0.38	2.09	1.69	1.19	1.66
2	0.14	...	0.32	1.81	1.35	1.29	1.22
3	0.12	...	0.33	1.58	0.89	1.48	0.79
4	0.09	...	0.20	1.16	0.47	1.21	0.46
5	0.14	0.31	0.52	2.21	1.43	1.89	1.25
6	0.12	0.18	0.32	1.67	0.89	1.56	0.82
7	0.11	0.14	0.24	1.46	0.70	1.41	0.51
8	0.10	0.11	0.17	1.24	0.54	1.25	0.53
9	0.12	...	...	1.52	0.90	1.40	0.78
10	0.06	...	...	0.83	0.39	0.96	0.30
11	0.15	0.66	...	2.12	2.23	0.31	1.87
12	0.16	0.40	...	2.31	1.93	1.53	0.87
13	0.15	0.75	...	1.60	1.39	1.05	1.18
14	0.11	0.00	...	0.70	0.70	0.49	0.52
15	0.13	0.00	...	1.44	1.14	0.50	1.20
Average	0.12	0.36	0.29	1.61	1.14	1.30	1.01

[a]RMSE, root-mean-square error.

characterized by exponential $K(h)$ function, for which the formula of *Baker* [1995, 2000] provides exact values of the Darcian means. In this case the Darcian means K_{DAR} computed numerically from the solution of the steady state problem are in perfect agreement with K_{BAKER} (RMSE of the order of 10^{-5}), which confirms the accuracy of the numerical method used to compute K_{DAR}. On the other hand, K_{NEW} performs better than K_{BAKER} for soils 11 and 13, characterized by a distinct air-entry pressure. This observation is consistent with the results shown by *Baker et al.* [1999] for soil 13. The method of *Gastó et al.* [2002] also gave a small value of the average RMSE, between the values obtained for K_{NEW} and K_{BAKER}. The other averaging methods produce significantly larger errors. It should be noted, however, that K_{GEOM} and K_{INT} seem to have considerable advantage over K_{ARIT} and K_{UPS} for fine-textured soils (soils 3, 4, 7, 8 and 10), which explains the recommendation for K_{GEO} by *Haverkamp and Vauclin* [1979].

[32] More insights into the performance of various methods can be gained from Table 3. It shows the values of RMSE computed for the ensemble of soils for the three types of flow (infiltration, drainage, and capillary rise) and three different ranges of grid block sizes Δz (small, medium, and large). Again, one can see that the methods based on the steady state solutions give in general much smaller errors that the simple averaging methods (K_{ARIT}, K_{GEOM}, K_{UPS}, and K_{INT}). Overall, K_{NEW} generated the smallest values of RMSE for all three ranges of Δz. As far as the performance for various types of flow is considered, K_{NEW} is more accurate than either K_{GASTO} or K_{BAKER} for infiltration and capillary rise, while for drainage it is inferior to K_{GASTO} but still superior to K_{BAKER}. It should be remembered, however, that this order of accuracy is based on averaged results, and can be different for some particular cases.

[33] Table 3 shows that for specific conditions even simple averaging methods can be quite accurate. K_{INT} is very accurate for small Δz and moderately accurate for medium Δz. Indeed, K_{INT} was recommended by some authors as the best approximation method for infiltration on relatively fine numerical grids [*Miller et al.*, 1998; *Belfort and Lehmann*, 2005]. For large Δz, K_{UPS} seems to be the most accurate of the simple approximations. K_{UPS} is also an accurate estimation for drainage flow, since in this case it corresponds to K_U, which is the correct limit value for the internodal conductivity for drainage, for both large and small Δz (see section 3.1). For the capillary rise, on the other hand, K_{UPS} corresponds to K_L, which is outside the limit values of the internodal conductivity (K_{INT}, K_U). Thus for the capillary rise K_{UPS} produces the largest error, while K_{GEOM} and K_{INT} seem to be better approximations in this case.

[34] The two rightmost columns of Table 3 show the values of maximum and minimum error obtained with the corresponding method for the whole range of calculations. The extreme case is represented by the error of 10.5 orders of magnitude for K_{ARIT}, corresponding to the drainage in soil 12 with large Δz. Other simple methods can also underestimate or overestimate the internodal conductivity by several orders of magnitude, for a particular set of nodal pressures, Δz, and soil parameters. K_{BAKER} generated errors of over 4 orders of magnitude, but they were limited to soils 11 and 13. On the other hand, the largest error generated by K_{NEW} is only 1.5 order of magnitude (315% of relative error in the value of K_{AV}). K_{GASTO} is similarly accurate, but it should be noted that it cannot be applied to all soils.

5. Examples of Unsteady Flow Simulations

5.1. Numerical Implementation

[35] In order to evaluate the performance of the proposed averaging method for unsteady flow simulation it has been implemented in a numerical code solving the one-dimen-

Table 3. Average RMSE Values Obtained for the Ensemble of Soils for Various Ranges of Grid Sizes and Various Types of Flow

	RMSE							
	Δz			Flow Type				
Method	Small (1 mm, 1 cm, 2 cm)	Medium (10 cm, 20 cm, 50 cm)	Large (1 m, 10 m, 100 m)	Infiltration	Drainage	Capillary Rise	Minimum Observed Error (MINE)	Maximum Observed Error (MAXE)
K_{NEW}	0.04	0.13	0.17	0.04	0.22	0.11	−1.50	0.11
K_{BAKER}	0.07	0.38	0.49	0.11	0.51	0.49	−4.30	4.47
K_{GASTO}	0.33	0.22	0.19	0.33	0.09	0.26	−1.24	1.60
K_{ARI}	1.13	1.33	2.17	0.86	2.57	1.74	−2.89	10.50
K_{GEOM}	0.84	0.89	1.55	1.26	1.29	0.77	−5.38	5.40
K_{UPS}	1.34	1.44	1.10	1.04	0.27	1.96	−6.05	8.18
K_{INT}	0.09	0.62	1.68	0.57	1.90	0.64	−3.23	8.55

Table 4. Results of the Numerical Simulations for Test Problem 1

Method	ε_h (cm)	ε_Q (%)	Max($\Delta h/\Delta z$) [ ]	*MB* (%)	Time (s)
			Δz = 50 cm		
K_{NEW}	2.06E+2	−1.6	0	9.1E-12	0.69
K_{BAKER}	2.16E+2	+1.6	0	2.0E-6	1.05
K_{GASTO}	...	...	...	...	...
K_{ARIT}	1.38E+2	−15.8	0.195	4.5E-3	0.76
K_{GEOM}	3.48E+2	−99.4	0	5.5E-6	0.66
K_{UPS}	2.62E+2	+9.3	0	3.5E-14	0.67
K_{INT}	3.64E+2	−99.7	0	1.2E-1	0.95
			Δz = 20 cm		
K_{NEW}	1.07E+2	−1.6	0	3.1E-8	0.68
K_{BAKER}	1.40E+2	+2.1	0	3.9E-4	0.96
K_{GASTO}	1.49E+2	+3.3	0	2.1E-4	0.95
K_{ARIT}	1.24E+2	−2.3	0.130	1.6E-5	1.22
K_{GEOM}	3.83E+2	−93.8	0	7.8E-7	1.29
K_{UPS}	1.85E+2	+5.6	0	1.3E-4	0.87
K_{INT}	2.05E+2	−32.4	0.117	6.0E-3	1.31
			Δz = 10 cm		
K_{NEW}	6.71E+1	−1.6	0	8.0E-13	1.04
K_{BAKER}	1.01E+2	+0.9	0	4.5E-4	0.96
K_{GASTO}	8.48E+1	−1.2	0	9.8E-7	1.30
K_{ARIT}	1.01E+2	−0.2	0.019	2.5E-7	0.96
K_{GEOM}	3.59E+2	−77.8	0.430	1.4E-5	0.94
K_{UPS}	1.43E+2	+3.7	0	1.1E-8	1.03
K_{INT}	9.44E+1	−9.3	0.101	4.4E-2	2.08
			Δz = 5 cm		
K_{NEW}	3.55E+1	−1.6	0	5.1E-8	16.8
K_{BAKER}	7.35E+1	+0.1	0	8.0E-8	27.5
K_{GASTO}	6.16E+1	−1.1	0	4.8E-6	26.9
K_{ARIT}	9.04E+1	+0.1	0.004	1.4E-8	15.5
K_{GEOM}	2.95E+2	−51.3	0.264	2.9E-3	19.4
K_{UPS}	1.19E+2	+2.4	0	1.3E-8	17.5
K_{INT}	3.61E+0	−2.9	0.160	9.3E-6	19.2
			Δz = 1 cm		
K_{NEW}	2.18E+1	−0.3	0	3.7E-4	18.6
K_{BAKER}	2.98E+1	−0.2	0	1.2E-4	30.2
K_{GASTO}	2.75E+1	−0.2	0	4.8E-6	42.4
K_{ARIT}	4.41E+1	+0.2	0	5.6E-9	17.2
K_{GEOM}	2.92E+1	+0.9	0	1.1E-4	35.2
K_{UPS}	6.32E+1	−0.4	0	1.9E-5	16.7
K_{INT}	2.67E+1	−0.4	0	5.9E-5	17.5

sional unsaturated flow equation, based on the mass-conservative approach of *Celia et al.* [1990]. The domain is discretized with N nodes, in such a manner that the outermost nodes are located at the physical boundaries of the domain. Then finite volumes are built around each of the nodes, with interfaces located at midpoints between adjacent nodes. The discrete analog of RE is as follows:

$$V_i \frac{\theta_i^{j+1} - \theta_i^j}{\Delta t} + S_{i+1/2}\, q_{i+1/2}^{j+1} - S_{i-1/2}\, q_{i-1/2}^{j+1} = 0 \tag{25a}$$

with

$$q_{i+1/2}^{j+1} = -K_{AV}^{j+1}\left(\frac{h_{i+1}^{j+1} - h_i^{j+1}}{\Delta z} - \gamma\right), \tag{25b}$$

where j is the time step index, i is the node index, V_i is the volume of the cell associated with node i, q denote internodal fluxes and $S_{i\pm1/2}$ are the interfacial areas between adjacent finite volumes (for flow in Cartesian coordinates, $S_{i\pm1/2}$ is equal to 1). The nonlinear equation for each time step (25a) is solved iteratively by the Newton method [e.g., *Miller et al.*, 1998], which appears to be more robust than the Picard method commonly used in numerical solvers of RE [e.g., *Celia et al.*, 1990; *Šimůnek et al.*, 1998; *van Dam and Feddes*, 2000]. The convergence criterion is specified in terms of the maximum allowable difference in the potential heads between two subsequent iterations. In all simulations except the reference solutions the error tolerance was set to (0.1 cm + 0.01$|h|$), while for the reference solutions it was decreased 10 times. The time step size was adjusted according to the performance of the nonlinear solver [*Šimůnek et al.*, 1998; *van Dam and Feddes*, 2000], in such a way that if the number of iterations is smaller than 3 then the step size is multiplied by 1.25 and when the number of iterations is higher than 7 the time step is divided by 1.25. Moreover, the maximum and minimum allowable time step sizes are specified.

[36] Numerical solution of RE requires multiple evaluations of the nonlinear functions of water potential, i.e., $\theta(h)$, $K(h)$, and for K_{INT}, K_{BAKER}, and K_{NEW}, also $\Phi(h)$. An efficient approach is to interpolate the values of these functions from a precomputed table [*Šimůnek et al.*, 1998; *Miller et al.*, 1998]. In the examples shown below, we used linear interpolation, with the interpolation nodes nonuniformly spaced, to obtain greater density in the range of greater variability of the functions (for water potential head close to 0 or to the air-entry pressure head). Preliminary tests with Hermite spline [*Miller et al.*, 1998] showed convergence problems for test problems 1 and 2.

[37] The overall efficiency of the numerical solution of RE depends on multiple factors. While the scheme presented here performed well in all test cases, further improvement can be possibly achieved by using more advanced time-integration and time stepping schemes, as shown by *Miller et al.* [1998]. A detailed examination of the performance of the proposed approach combined with more sophisticated discretization schemes is beyond the scope of this paper.

5.2. Test Problem 1: Infiltration in Sand With Constant Head Boundary Condition

[38] The first test concerns infiltration into a 5-m-deep dry sand layer. The $S_E(h)$ and $K_{REL}(h)$ functions correspond to soil 5 (Table 1). The saturated conductivity is K_S = 21 cm/h. The volumetric water content θ is related to the effective saturation S_E by the formula $S_E = (\theta - \theta_R)/(\theta_S - \theta_R)$, where the saturated water content θ_S = 0.430 and the residual water content θ_R = 0.045. The initial condition is specified as $h(z, t = 0) = -750$ cm (θ = 0.069). At the upper boundary a constant potential head is applied $h = -7.5$ cm, which correspond to near-saturated conditions (θ = 0.422), while the lower boundary is maintained at the initial potential head. The reference numerical solution is obtained with K_{INT} and Δz = 0.05 cm. For such a fine discretization all examined conductivity averaging methods lead to very similar results. The results of simulations for coarser discretizations are shown in Table 4. The solutions are compared with the reference one in terms of the norm of the error in water potential head ε_h and the error in the cumulative infiltration, ε_Q, which are computed as

$$\varepsilon_h = \left(\frac{1}{N}\sum_{i=1}^{N}\left(h_i - h_{i,ref}\right)^2\right)^{0.5}, \tag{26a}$$

$$\varepsilon_Q = \left(1 - \frac{Q_{in}}{Q_{in,ref}}\right)\cdot 100\%, \tag{26b}$$

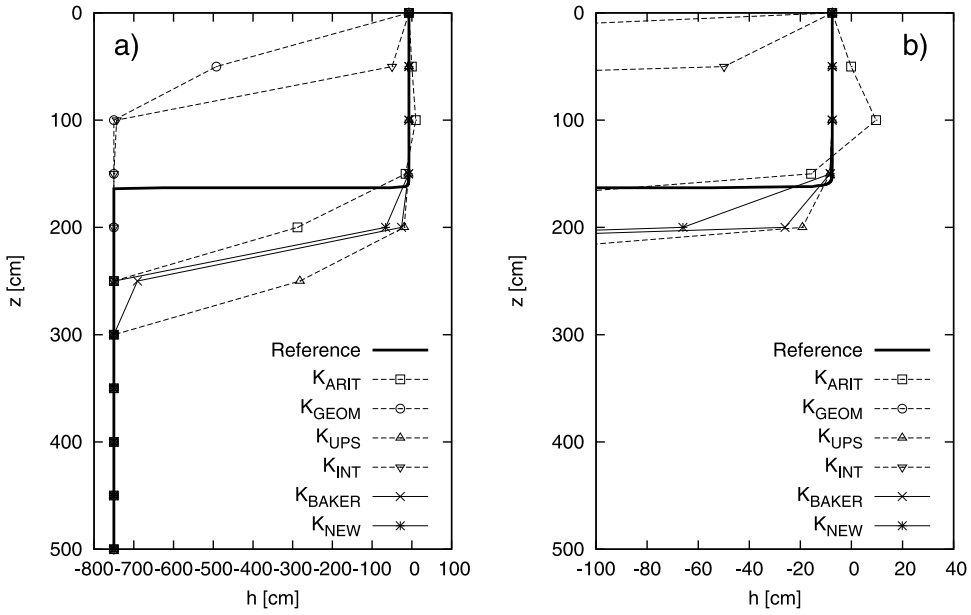

Figure 6. Test problem 1. (a) Water potential head profiles after 3 h of infiltration for Δz = 50 cm, obtained with various averaging methods. (b) Zoomed profiles, showing the oscillation obtained with K_{ARIT}.

where N is the number of nodes for the considered discretization, h_i is the water potential at node i obtained from the considered solution, $h_{i,ref}$ is the potential head at the same node obtained from the reference solution, Q_{in} is the total amount of infiltrated water obtained by numerical integration of the infiltration flux for the considered solution, and $Q_{in,ref}$ is the corresponding value obtained from the reference solution. As an additional measure of the quality of solution we provide information on the maximum gradient of the water potential head in the domain, max $(\Delta h/\Delta z)$. For the considered case it should not exceed zero; positive values indicate unphysical oscillations. Moreover, information on mass balance and computational time is provided. The mass balance error MB is computed as

$$MB = \frac{\left|VOL_{final} - VOL_{init} - Q_{in} + Q_{out}\right|}{\min\left(\left|VOL_{final} - VOL_{init}\right|, \left|Q_{in} - Q_{out}\right|\right)}, \qquad (27)$$

where VOL_{final} and VOL_{init} denote the final and initial amount of water in the domain and Q_{in} and Q_{out} are cumulative fluxes at the top and the bottom of the layer. The simulation time is the clock time, which includes the time necessary to generate the interpolation table (with $\Phi(h)$ values in the case of K_{INT}, K_{BAKER} and K_{NEW}). In this case an interpolation table with 50 nodes was used (h from −7.3 cm to −1000 cm), while the time step was allowed to vary from 1e-15 to 0.01 h. All simulations reported in this paper were carried out on a Pentium 4 2.00-GHz machine with 1 GB RAM.

[39] Table 4 shows very large differences between the solutions obtained with various averaging methods on coarse grids (Δz = 50 cm and 20 cm). A visual illustration is provided by Figure 6, where the water potential head profiles are compared for Δz = 50 cm. K_{INT} and K_{GEOM} underestimate the position of the wetting front, while other methods overestimate it. The best result with respect to the position of the wetting front is obtained with K_{ARIT}, which is also confirmed by the lowest value of ε_h. However, this method produces unphysical overshoot of the potential head behind the wetting front. This oscillation is better seen in Figure 6b, where the horizontal axis scale is enlarged. In this case the overshoot is relatively small; much larger oscillations were reported for vertical infiltration with K_{ARIT} [*Baker et al.*, 1999; *Baker*, 2006]. Nevertheless, K_{ARIT} predicts positive potential heads in the domain, which are outside the range resulting from the initial and boundary conditions. K_{NEW} and K_{BAKER} produce oscillation-free solutions, very close to each other. While they both overestimate the position of the wetting front, the error is smaller than for all other methods, except K_{ARIT}. Note also that only K_{NEW} and K_{BAKER} predict accurate amount of infiltration even on the coarsest grid (for this case, K_{GASTO} produced negative values of conductivity and the solution did not converge). As the grid is refined, the errors diminish significantly. Still, oscillations appear in solutions obtained with K_{ARIT}, K_{GEOM}, and K_{INT} even for Δz = 5 cm, as shown by positive gradients of potential head in Table 4. Despite the oscillations, K_{ARIT} is able to predict the amount of infiltrated water with slightly higher accuracy than other methods for Δz = 5 cm and 10 cm. For all grids K_{NEW} gives the best or second best approximations of the reference solution in terms of ε_h, while ε_Q is also relatively small. The differences in computational time between various approaches become more pronounced only for the finest discretizations (Δz = 5 cm and 1 cm). In all cases simulations with K_{NEW} required similar time as with K_{ARIT}, while K_{GASTO} and K_{BAKER} required significantly more time on finer grids (up to over 100% for K_{GASTO} with Δz = 1 cm). The mass balance was satisfied for all methods, with errors lower than 1%, which is also the case for all the following examples. Note, however, that even a perfect mass balance

Table 5. Results of the Numerical Simulations for Test Problem 2

Method	ε_h (cm)	ε_Q (%)	Min($\Delta h/\Delta z$) [ ]	*MB* (%)	Time (s)
			Δz = 50 cm		
K_{NEW}	3.80E+0	−5.6	0	2.8E-1	0.64
K_{BAKER}	4.66E+0	−6.3	0	2.9E-1	0.80
K_{GASTO}	9.80E+0	−2.2	0	2.9E-1	0.70
K_{ARIT}	1.05E+1	+1.8	−0.687	6.6E-2	0.70
K_{GEOM}	5.27E+0	−2.2	−0.397	3.0E-1	0.64
K_{UPS}	5.06E+0	−6.6	0	2.9E-1	0.61
K_{INT}	6.77E+0	−1.3	−0.507	2.5E-1	0.63
			Δz = 20 cm		
K_{NEW}	4.97E-1	−1.1	0	2.6E-1	0.71
K_{BAKER}	1.28E+0	+2.0	0	2.8E-1	0.76
K_{GASTO}	1.58E+0	−2.1	0	2.9E-1	0.70
K_{ARIT}	1.39E+0	+0.1	−0.315	1.1E-1	0.66
K_{GEOM}	7.74E-1	−0.2	−0.164	3.0E-1	0.74
K_{UPS}	1.84E+0	−2.4	0	2.9E-1	0.67
K_{INT}	9.31E-1	−0.1	−0.213	3.1E-1	0.90
			Δz = 10 cm		
K_{NEW}	2.99E-1	+0.1	0	2.7E-1	0.82
K_{BAKER}	4.36E-1	−0.6	0	2.9E-1	0.93
K_{GASTO}	3.96E-1	−0.4	0	3.0E-1	0.86
K_{ARIT}	2.09E-1	+0.3	0	3.1E-1	0.78
K_{GEOM}	1.22E-1	+0.1	0	3.1E-1	0.80
K_{UPS}	9.01E-1	−1.0	0	3.0E-1	0.77
K_{INT}	1.36E-1	+0.1	0	2.7E-1	1.27
			Δz = 5 cm		
K_{NEW}	1.92E-1	+0.3	0	2.8E-1	1.02
K_{BAKER}	1.44E-1	−0.1	0	3.0E-1	1.23
K_{GASTO}	1.22E-1	−0.1	0	3.0E-1	1.42
K_{ARIT}	5.71E-2	+0.1	0	3.0E-1	0.90
K_{GEOM}	4.02E-2	+0.1	0	2.9E-1	0.93
K_{UPS}	4.62E-1	−0.5	0	3.0E-1	0.89
K_{INT}	4.01E-2	0.0	0	2.4E-1	1.73
			Δz = 1 cm		
K_{NEW}	2.68E-2	+0.2	0	2.8E-1	2.51
K_{BAKER}	2.69E-2	0.0	0	1.9E-1	3.81
K_{GASTO}	3.32E-2	+0.1	0	2.9E-1	2.75
K_{ARIT}	2.92E-2	+0.1	0	2.9E-1	1.91
K_{GEOM}	2.96E-2	+0.1	0	2.9E-1	2.30
K_{UPS}	1.31E-1	0.0	0	2.9E-1	1.99
K_{INT}	1.94E-2	0.0	0	1.6E-1	2.52

does not ensure accurate estimation of the amount of infiltrated water.

5.3. Test Problem 2: Drainage in Sand

[40] In the second test drainage in the same sand layer was simulated. Initially the layer was assumed quasi-saturated with a uniform distribution of the water potential head h (z, t = 0) = −7.5 cm. This value was kept constant at the lower boundary, while at the upper boundary a no-flow condition (q = 0) was imposed. In this case a dense interpolation table with 1000 nodes covering the values of the potential head from −7.5 to −200 cm was required. The maximum allowable time step was 0.1 h. The results of the simulations are listed in Table 5. The presented parameters are similar to those from test problem 1, ε_Q representing the error in cumulative amount of drained water, and the minimum value of the potential head gradient min ($\Delta h/\Delta z$) indicating the magnitude of oscillations (only nonnegative gradients are physically admissible). Figures 7a and 7b show the potential head profiles obtained on the coarsest grid (Δz = 50 cm) for the simple averaging methods and for the averaging methods based on Darcian means, respectively. It can be seen that K_{ARIT}, K_{GEOM}, and K_{INT} produce large oscillations in the potential head profile, while all of them predict the amount of drained water with remarkably high accuracy (better than K_{NEW} and K_{BAKER}). On the other hand, both K_{NEW} and K_{BAKER} lead to solutions relatively close to the reference one. Again, such a coarse discretization is outside the range of applicability of K_{GASTO}. While a convergent solution was obtained with this method, it is clearly inaccurate. For finer grids, however, K_{GASTO} showed similar behavior to K_{NEW} and K_{BAKER}. K_{NEW} produced the best or second best results in terms of ε_h for all cases except Δz = 5 cm. For this discretization K_{NEW} is inferior to all other methods, except K_{UPS}, both in terms of ε_h and ε_Q, albeit the differences are not large. It should be noted that in the considered case K_{ARIT}, K_{GEOM} and K_{INT} outperform all three methods based on Darcian mean (K_{NEW}, K_{GASTO}, and K_{BAKER}), while for Δz = 1 cm all methods produce rather similar results.

5.4. Test Problem 3: Infiltration in Sand With Variable Boundary Condition

[41] This example is taken from the paper by *van Dam and Feddes* [2000]. A 40-cm-deep sandy soil layer is considered, with van Genuchten–Mualem parameters α = 0.0245 cm^{-1}, n = 1.507, θ_S = 0.43, θ_R = 0.01, K_S = 17.5 cm/d, and the connectivity parameter L = −0.14. Initially the soil is very dry with θ = 0.1 (h = −832.5 cm). At the surface a constant infiltration flux equal to 100 cm/d is imposed, until the surface grid block becomes saturated. From this time on, a constant head h = 0 cm is imposed at the surface, and the infiltration flux gradually decreases.

[42] The reference numerical solution for this case was obtained on a fine grid of 0.05 cm. For such a fine discretization, virtually the same results were produced with K_{INT} and K_{ARIT}. The reference solution predicts the total amount of infiltration equal to 3.69 cm, with ponding condition occurring at t = 0.006 day. These values are somewhat different from the reference solution presented by *van Dam and Feddes* [2000] for Δz = 0.1 cm, but they were confirmed by simulation with independent numerical code HYDRUS-1D [*Šimůnek et al.*, 1998]. HYDRUS-1D is based on the finite element discretization with mass-lumping and arithmetic averaging of the nodal conductivites, which results in a scheme equivalent to K_{ARIT}. Indeed, very good agreement was observed between the solutions from HYDRUS-1D and from the author's code with K_{ARIT} for the whole range of discretizations, including the reference solution. The discrepancy with respect to the results of *van Dam and Feddes* [2000] might be partly explained by the fact that in their numerical scheme the values of hydraulic conductivities were not updated in the iteration procedure, in contrast to the author's code and HYDRUS-1D.

[43] In order to evaluate the performance of various averaging schemes, simulations were carried out with Δz = 1 cm, 5 cm, and 10 cm. The interpolation table had 50 entries, and the maximum time step was 0.001 day. In Table 6 the cumulative infiltration Q_{in} and the time to ponding t_p is shown for each solution, together with the mass balance error and the simulation time. It can be seen that K_{NEW} offers a significant improvement over K_{ARIT}, especially for coarser grids. In contrast to the results reported by *van Dam and Feddes* [2000] K_{ARIT} seem to give nonnegligible errors even for Δz = 1 cm. K_{INT} gives virtually the same results as K_{NEW}, since for capillary

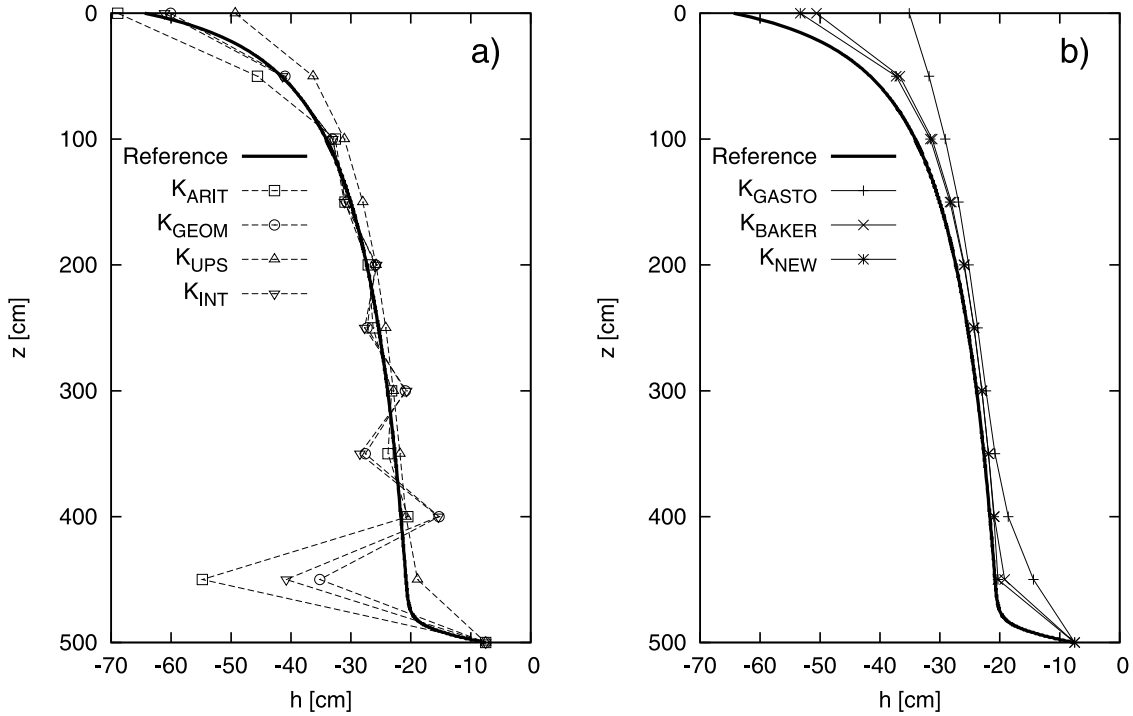

Figure 7. Test problem 2: Water potential head profiles after 30 h of drainage for $\Delta z = 50$ cm, obtained (a) with the simple averaging methods and (b) with the methods based on Darcian means.

dominated flow $K_{NEW} \rightarrow K_{INT}$, according to equation (11). The largest errors were produced by the upstream mean K_{UPS}. This case is outside the domain of applicability of K_{GASTO} and K_{BAKER}.

5.5. Test Problem 4: Evaporation From Sand With Variable Boundary Condition

[44] This example is also taken from *van Dam and Feddes* [2000]. The same soil profile is considered. Initially the soil is moderately wet ($\theta = 0.191$, $h = -200$ cm) and the initial value of the potential head is maintained at the lower boundary. At the surface a constant evaporation rate of 0.5 cm/d is applied until the top node dries up to the value of potential head $h_{crit} = -137{,}700$ cm. At this moment the boundary condition is changed to constant head $h = h_{crit}$, and consequently the actual evaporation rate decreases. The same set of numerical simulations as in the previous example was carried out. Again, in this case the reference solutions ($\Delta z = 0.05$ cm) provided by HYDRUS-1D and the author's code with K_{INT} and K_{ARIT} are very close to each other, yielding the cumulative evaporation of 0.89 cm and the time at which the surface dries up to the value of h_{crit} equal to 0.51 day. These values are different from the reference values shown in the paper by *van Dam and Feddes* [2000], while for $\Delta z = 1$ cm and 5 cm both HYDRUS-1D and the author's code with K_{ARIT} produced results very close to the ones from the mentioned paper.

[45] The numerical simulations were performed with interpolation table containing 100 entries covering the h range up to h_{crit}. The maximum allowable time step was 0.1 day. In the comparison between various averaging methods we used similar criteria as in test problem 3, including the cumulative evaporation Q_{ev} and the time to drying t_d. They are listed in Table 7, together with information on mass balance and simulation time. In this case K_{ARIT} gives significant error even for $\Delta z = 1$ cm, while K_{NEW} and K_{INT} lead to solutions much more accurate than K_{ARIT} for all grid sizes. For the considered $K(h)$ function and Δz values K_{NEW} computed from equation (17) closely approaches K_{INT}, giving practically the same results.

6. Discussion

6.1. Comparison With Existing Methods

[46] The results of calculations presented in sections 4 and 5 show that the most important advantage of the

Table 6. Results of the Numerical Simulations for Test Problem 3

Method	Q_{in} (cm)	t_p (d)	MB (%)	Time (s)
		$\Delta z = 10$ cm		
K_{NEW}	3.12	0.017	8.3E-1	1.09
K_{ARIT}	5.98	0.032	4.2E-3	0.95
K_{GEOM}	2.30	0.017	3.7E-1	0.75
K_{UPS}	7.13	0.041	8.7E-4	0.73
K_{INT}	3.11	0.017	8.4E-1	0.71
		$\Delta z = 5$ cm		
K_{NEW}	3.46	0.009	2.0E-1	0.72
K_{ARIT}	4.88	0.020	2.3E-3	0.71
K_{GEOM}	2.91	0.008	1.0E+0	0.67
K_{UPS}	5.82	0.027	1.1E-3	0.71
K_{INT}	3.46	0.009	2.0E-1	0.72
		$\Delta z = 1$ cm		
K_{NEW}	3.68	0.006	4.9E-4	1.20
K_{ARIT}	3.88	0.009	1.3E-3	1.98
K_{GEOM}	3.66	0.002	6.2E-2	1.48
K_{UPS}	4.29	0.012	4.5E-4	0.85
K_{INT}	3.68	0.006	4.9E-4	1.01

Table 7. Results of the Numerical Simulations for Test Problem 4

Method	Q_{ev} (cm)	t_d (d)	MB (%)	Time (s)
		Δz = 10 cm		
K_{NEW}	1.35	2.24	3.8E-2	0.90
K_{ARIT}	2.48	4.84	3.8E-2	0.90
K_{GEOM}	1.07	2.08	3.1E-1	0.78
K_{UPS}	2.50	>5	5.4E-8	0.80
K_{INT}	1.35	2.24	3.8E-2	0.75
		Δz = 5 cm		
K_{NEW}	1.07	1.34	1.7E-1	0.83
K_{ARIT}	1.89	3.00	2.2E-2	0.69
K_{GEOM}	0.69	1.21	1.2E-1	0.82
K_{UPS}	2.10	3.57	9.1E-2	0.84
K_{INT}	1.07	1.35	9.5E-2	0.87
		Δz = 1 cm		
K_{NEW}	9.00	0.63	9.5E-1	0.95
K_{ARIT}	1.12	1.14	3.8E-2	0.80
K_{GEOM}	0.59	0.57	6.1E-1	0.83
K_{UPS}	1.26	1.41	6.3E-3	0.82
K_{INT}	8.90	0.68	4.3E-2	0.85

proposed method is its ability to produce relatively accurate results for a wide range of flow scenarios. This does not mean that the method is always superior to all the existing approaches. As shown in Tables 4–7, in many cases a similar or superior accuracy can be achieved using a simpler method. However, none of the simple averaging schemes (K_{ARIT}, K_{GEOM}, K_{UPS}, K_{INT}) is able to produce satisfactory results in all cases. For example, K_{INT} gave very good results for test problems 3 and 4, but produced very inaccurate solutions for test problem 1 with Δz = 20 and 50 cm, and oscillatory solutions (though accurate in terms of cumulative flux) for test problem 2 with Δz = 20 and 50. On the other hand K_{ARIT} produced solutions that were relatively accurate in terms of cumulative fluxes in test problems 1 and 2, but showed significant unphysical oscillations for coarser grids. In contrast, for test problems 3 and 4 K_{ARIT} was relatively inaccurate in terms of the cumulative fluxes even for Δz = 1 cm.

[47] Compared with the existing averaging methods based on Darcian mean concept (K_{BAKER} and K_{GASTO}), the proposed scheme offers a comparable accuracy, and slightly better efficiency in terms of computational times on finer grids (Tables 4 and 5). However, K_{GASTO} can be used only for the functions of Brooks-Corey and van Genuchten–Mualem (with the connectivity parameter L = 0.5), and cannot be used for arbitrarily large grid sizes. The method of *Baker* [2000] can be used for arbitrary Δz and theoretically for any type of $K(h)$ function, but requires inversion of the conductivity function to obtain $h(K)$, which in general can be done only numerically (although the use of an interpolation table could speed up the process). Moreover, the comparisons with steady state solutions shown in section 4 indicate that the for some particular soil types the errors generated by K_{BAKER} can be significantly larger than with the new approach [cf. *Baker et al.*, 1999].

[48] The results also show that when a sufficiently fine grid is used, the choice of averaging schemes does not affect significantly the accuracy of the solution. If this is the case, simple averaging schemes like K_{ARIT} can actually outperform more complex approaches based on the Darcian mean concept, and the latter ones do not offer any advantage (Table 5, Δz = 5 cm). However, it is difficult to estimate a priori what size of grid is sufficiently fine to obtain an accurate solution, independent of the averaging scheme. For instance, in the cases presented here, the "safe" value of Δz can be assumed as 1 cm for test problem 1 and 10 cm for test problem 2, while in test problems 3 and 4 significant differences occurred even for Δz = 1 cm, and diminished only in fine-scale solutions with Δz = 0.1 or 0.05 cm. Thus it seems convenient to use an averaging method which does not produce unphysical or largely inaccurate results even for coarser grids. An alternative approach would be to use a spatially adaptive numerical method with dynamic grid refinement, controlled by the estimation of spatial discretization error [e.g., *Miller et al.*, 2006]. Such an approach can be expected to be more accurate (especially in terms of the wetting or drying front position) than any coarse grid solution, albeit at the expense of additional algorithmic complexity.

6.2. Variably Saturated Flow

[49] An algorithm for computing internodal conductivities should also account for the case when a part of the grid block between two neighboring nodes is fully saturated, i.e., the water potential is positive (or greater than the air-entry pressure) at one of the nodes [e.g., *Pei et al.*, 2006]. In such a case it has been suggested to find an approximate position of the boundary between the saturated and unsaturated zone and to compute the average conductivity as the harmonic mean of the values for the saturated and unsaturated part [*Gastó et al.*, 2002]. In the saturated region it is assumed that the conductivity is constant and equal to K_S, while in the unsaturated region one of the available averaging methods is used. It should be noted that when the method proposed in this paper is used, there is no need to search for the position of the saturated-unsaturated interface, because the analysis of the steady state profiles presented in section 3 holds also when a part of the grid block is fully saturated. Let us consider, for instance, vertical infiltration when the potential head at the lower node is negative, while the potential at the upper node is at first equal to zero and then positive. The higher the potential at the upper node, the closer K_{AV} should be to K_S. Most of the averaging methods, however, will predict the same value of K_{AV} in the two cases, since the conductivity at the upper node remains equal to K_S as the potential increases from zero to a positive value. However, when the integrated mean K_{INT} is used, in the second case the value of K_{AV} will be closer to K_S, as results from equation (3d). Consequently, according to equation (11), the method proposed here should be able to reproduce the dependency of K_{AV} on the value of the positive potential at the upper node. A similar analysis holds for drainage and capillary rise. These considerations are confirmed by comparison with numerical solution of the steady flow problem for saturated-unsaturated conditions. The computations were carried out for soil 1, with Δz = {1 mm, 1 cm, 2 cm, 10 cm, 20 cm, 50 cm, 1 m, 10 m, 100 m} and h_U, h_L = {±1 mm, ±1 cm, ±10 cm, ±1 m, ±10 m, ±100 m} (in each case the nodal potentials had opposite signs). The resulting RMSE values were 0.04 for infiltration, 0.003 for drainage, and 0.2 for the capillary rise. Thus it seems that the method can be used in the whole range of the water potentials, including the positive ones.

6.3. Heterogeneous Soils

[50] While all the presented examples concerned homogenous media, the proposed method of computing K_{AV} can be used also for heterogeneous (layered) soils. For such type of media two approaches to spatial discretization can be distinguished. In the first one the nodes are located at material interfaces (boundaries of the layers). Thus the layer of soil between the adjacent nodes is always homogeneous [*Gastó et al.*, 2002]. The proposed method can be applied directly in this case, the only modification being that different $K(h)$ functions have to be used in different parts of the profile, while for a node located at the material interface the term $V_i\theta_i$ in equation (25a) should be split in two parts, corresponding to the two subregions of the finite volume. In the second case the nodes are placed in such a way that the material interfaces are located between them. In such a situation the method cannot be used directly, due to the existence of the discontinuity in $K(h)$ function. In order to find the approximate shape of the steady state profile one has to introduce an auxiliary variable h^* representing the water potential head at the material interface. The value of the interface potential can be computed from the flux continuity condition, i.e., assuming that the water fluxes at both sides of the interface should be equal. The flux continuity condition represents a nonlinear equation with respect to h^*. Its solution allows us to compute the water flux over the interface and consequently the average conductivity. This type of algorithm was used by *Desbarats* [1995], *Romano et al.* [1998], and *Brunone et al.* [2003]. *Desbarats* [1995] used an analytical solution of the steady flow equation for exponential $K(h)$ function to derive a Darcian type of approximation for K_{AV}, similar to the one of *Baker* [1995]. *Romano et al.* [1998] and *Brunone et al.* [2003] used geometric averaging to estimate the fluxes at both sides of the interface. Since the geometric mean is known to be inaccurate in many situation (see the examples above), one could expect some improvement if the method proposed in this paper were used in the framework of the approach of *Romano et al.* [1998] and *Brunone et al.* [2003]. A detailed evaluation of the performance of the proposed method for heterogeneous media is outside the scope of this paper and is a subject of ongoing research.

6.4. Multidimensional Problems

[51] The proposed method of conductivity averaging has been derived and was intended to be used for one-dimensional simulation. However, its application can be extended for some types of multidimensional problems. For a structured grid consisting of rectangular cells, a simple finite volume scheme similar to equations (25a) and (25b) can be used, resulting in well-known five-point stencil for 2-D flow and seven-point stencil for 3-D flow [e.g., *Gastó et al.*, 2002; *Szymkiewicz et al.*, 2008]. The fluxes in vertical directions can be approximated using the proposed method, while the horizontal fluxes are best approximated with the integrated mean K_{INT} [*Baker*, 2000; *Gastó et al.*, 2002]. This scheme is applicable for isotropic or orthotropic media (with off-diagonal components of the conductivity tensor equal to zero). The proposed method cannot be directly applied for unstructured meshes and anisotropic media. However, it seems clear that also in such cases the method of conductivity averaging should take into account the local balance of capillary and gravity forces, and the results presented here can provide some suggestions for the choice of the averaging method from the available schemes.

7. Conclusions

[52] A new method for approximating internodal conductivity in the numerical solution of one-dimensional unsaturated flow equation is proposed. The method is based on approximation of the steady state water potential head distribution between adjacent nodes, according to the Darcian mean concept. Compared with the existing Darcian approaches, the proposed method shows a similar performance and a wider range of applicability. Numerical simulation showed that Darcian methods are particularly advantageous for coarser grids, ensuring oscillation-free and relatively accurate solutions even for large spatial steps. While simple averaging schemes, like arithmetic mean, show similar or even superior performance on sufficiently fine grids, the critical grid size for which they lead to acceptable results is difficult to establish a priori, and depends very much on the conditions of flow and type of soil.

[53] The proposed method makes use of the integrated mean of the hydraulic conductivity, which requires additional preprocessing and implementation of an interpolation procedure. Moreover, the application of the method for multidimensional cases is generally limited to simple rectangular grids. Despite these limitations, the method seems to be, at least in some cases, a useful alternative to the existing averaging methods, as it can be applied for arbitrary type of conductivity function and arbitrary large grid sizes. Finally, it should be noted that the proposed method can be used for relatively accurate estimation of steady state water fluxes across layers of soils or other porous materials.

[54] **Acknowledgments.** The author wish to thank three anonymous reviewers for their valuable suggestions and comments.

References

Baker, D. L. (1995), Darcian weighted interblock conductivity means for vertical unsaturated flow, *Ground Water*, *33*, 385–390, doi:10.1111/j.1745-6584.1995.tb00294.x.

Baker, D. L. (2000), A Darcian integral approximation to interblock hydraulic conductivity means in vertical infiltration, *Comput. Geosci.*, *26*, 581–590, doi:10.1016/S0098-3004(99)00129-6.

Baker, D. L. (2006), General validity of conductivity means in unsaturated flow, *J. Hydrol. Eng.*, *11*(6), 526–538, doi:10.1061/(ASCE)1084-0699(2006)11:6(526).

Baker, D. L., M. E. Arnold, and H. D. Scott (1999), Some analytic and approximate Darcian means, *Ground Water*, *37*, 532–538, doi:10.1111/j.1745-6584.1999.tb01139.x.

Belfort, B., and F. Lehmann (2005), Comparison of equivalent conductivities for numerical simulation of one-dimensional unsaturated flow, *Vadose Zone J.*, *4*, 1191–1200, doi:10.2136/vzj2005.0007.

Brooks, R. H., and A. T. Corey (1964), Hydraulic properties of porous media, *Hydrol. Pap. 3*, Colo. State Univ., Fort Collins.

Brunone, B., M. Ferrante, N. Romano, and A. Santini (2003), Numerical simulations of one-dimensional infiltration into layered soils with the Richards' equation using different estimates of the interlayer conductivity, *Vadose Zone J.*, *2*, 193–200, doi:10.2113/2.2.193.

Caputo, M. C., and J. R. Nimmo (2005), Quasi-steady centrifuge method for unsaturated hydraulic properties, *Water Resour. Res.*, *41*, W11504, doi:10.1029/2005WR003957.

Carsel, R. F., and R. S. Parrish (1988), Developing joint probability distribution of soil water retention characteristics, *Water Resour. Res.*, *24*(5), 755–769, doi:10.1029/WR024i005p00755.

Celia, M. A., E. T. Bouloutas, and R. L. Zarba (1990), A general mass-conservative numerical solution for the unsaturated flow equation, *Water Resour. Res.*, *26*, 1483–1496.

Desbarats, A. J. (1995), An interblock conductivity scheme for finite difference models of steady unsaturated flow in heterogeneous media, *Water Resour. Res.*, *31*(11), 2883–2889, doi:10.1029/95WR02429.

Forsyth, P. A., Y. S. Wu, and K. Pruess (1995), Robust numerical methods for saturated-unsaturated flow with dry initial conditions in heterogeneous media, *Adv. Water Resour.*, *18*, 25–38, doi:10.1016/0309-1708(95)00020-J.

Fuentes, C., R. Haverkamp, and J.-Y. Parlange (1992), Parameter constraints on closed-form soil-water relationships, *J. Hydrol.*, *134*, 117–142, doi:10.1016/0022-1694(92)90032-Q.

Gardner, W. R. (1958), Some steady-state solutions of the unsaturated moisture flow equation with application to evaporation from a water table, *Soil Sci.*, *85*, 228–232.

Gastó, J. M., J. Grifoll, and Y. Cohen (2002), Estimation of internodal permeabilities for numerical simulation of unsaturated flows, *Water Resour. Res.*, *38*(12), 1326, doi:10.1029/2002WR001529.

Haverkamp, R., and M. Vauclin (1979), A note on estimating finite difference interblock hydraulic conductivity values for transient unsaturated flow problems, *Water Resour. Res.*, *15*, 181–187, doi:10.1029/WR015i001p00181.

Haverkamp, R., M. Vauclin, J. Touma, P. J. Wierenga, and G. Vachaud (1977), A comparison of numerical simulation models for one-dimensional infiltration, *Soil Sci. Soc. Am. J.*, *41*, 285–294.

Helmig, R., and R. Huber (1996), Comparison of Galerkin-type discretization techniques for two-phase flow in heterogeneous porous media, *Adv. Water Resour.*, *21*(8), 697–711, doi:10.1016/S0309-1708(97)00023-7.

Kutílek, M., and D. R. Nielsen (1994), *Soil Hydrology*, Catena, Cremlingen, Germany.

Lassabatere, L., R. Angulo-Jaramillo, J. M. Soria Ugalde, R. Cuenca, I. Braud, and R. Haverkamp (2006), Beerkan estimation of soil transfer parameters through infiltration experiments—BEST, *Soil Sci. Soc. Am. J.*, *70*, 521–532, doi:10.2136/sssaj2005.0026.

Manzini, G., and S. Ferraris (2004), Mass-conservative finite volume methods on 2-D unstructured grids for the Richards' equation, *Adv. Water Resour.*, *27*, 1199–1215, doi:10.1016/j.advwatres.2004.08.008.

Miller, C. T., G. A. Williams, C. T. Kelley, and M. D. Tocci (1998), Robust solution of Richards' equation for nonuniform porous media, *Water Resour. Res.*, *34*, 2599–2610, doi:10.1029/98WR01673.

Miller, C. T., C. Abhishek, and M. W. Farthing (2006), A spatially and temporally adaptive solution of Richards' equation, *Adv. Water Resour.*, *29*(4), 525–545, doi:10.1016/j.advwatres.2005.06.008.

Mualem, Y. (1976), A new model for predicting the hydraulic conductivity of unsaturated porous media, *Water Resour. Res.*, *12*, 513–522, doi:10.1029/WR012i003p00513.

Oldenburg, C. M., and K. Pruess (1993), On numerical modeling of capillary barriers, *Water Resour. Res.*, *29*(4), 1045–1056, doi:10.1029/92WR02875.

Pei, Y., J. Wang, Z. Tian, and J. Yu (2006), Analysis of interfacial error in saturated-unsaturated flow models, *Adv. Water Resour.*, *29*, 515–524, doi:10.1016/j.advwatres.2005.06.007.

Romano, N., B. Brunone, and A. Santini (1998), Numerical analysis of one-dimensional unsaturated flow in layered soils, *Adv. Water Resour.*, *21*, 315–324, doi:10.1016/S0309-1708(96)00059-0.

Ross, P. (2003), Modeling soil water and solute transport—Fast, simplified numerical solutions, *Agron. J.*, *95*, 1352–1361.

Schaap, M. G., and F. J. Leij (2000), Improved prediction of unsaturated hydraulic conductivity with the Mualem–van Genuchten model, *Soil Sci. Soc. Am. J.*, *64*, 843–851.

Šimůnek, J., M. Sejna, and M. van Genuchten (1998), HYDRUS-1D software package for simulating the one-dimensional movement of water, heat and multiple solutes in variably saturated media, U.S. Salinity Lab., Agric. Res. Serv., U.S. Dep. of Agric., Riverside, Calif.

Srivastava, R., and A. Guzman-Guzman (1995), Analysis of hydraulic conductivity averaging schemes for one-dimensional, steady-state unsaturated flow, *Ground Water*, *33*, 946–952, doi:10.1111/j.1745-6584.1995.tb00040.x.

Szymkiewicz, A. (2007), Numerical simulation of one-dimensional two-phase flow in porous media, *Arch. Hydro Eng. Environ. Mech.*, *54*, 117–136.

Szymkiewicz, A., J. Lewandowska, R. Angulo-Jaramillo, and J. Butlańska (2008), Two-scale modeling of unsaturated water flow in a double-porosity medium under axisymmetric conditions, *Can. Geotech. J.*, *45*, 238–251, doi:10.1139/T07-096.

van Dam, J. C., and R. A. Feddes (2000), Numerical simulation of infiltration, evaporation and shallow groundwater levels with the Richards equation, *J. Hydrol.*, *233*, 72–85, doi:10.1016/S0022-1694(00)00227-4.

van Genuchten, M. (1980), A closed form equation for predicting the hydraulic conductivity of unsaturated soils, *Soil Sci. Soc. Am. J.*, *44*, 892–898.

Warrick, A. W. (1991), Numerical approximation of Darcian flow through unsaturated soil, *Water Resour. Res.*, *27*, 1215–1222, doi:10.1029/91WR00093.

Warrick, A. W. (2003), *Soil Water Dynamics*, Oxford Univ. Press, New York.

Warrick, A. W., and T.-C. J. Yeh (1991), One-dimensional, steady vertical flow in a layered soil profile, *Adv. Water Resour.*, *13*, 207–210, doi:10.1016/0309-1708(90)90042-3.

Zaidel, J., and D. Russo (1992), Estimation of finite difference interblock conductivities for simulation of infiltration into initially dry soils, *Water Resour. Res.*, *28*, 2285–2295, doi:10.1029/92WR00914.

Zhang, X., and J. Ewen (2000), Efficient method for simulating gravity-dominated water flow in unsaturated soils, *Water Resour. Res.*, *36*(9), 2777–2780, doi:10.1029/2000WR900182.

A. Szymkiewicz, Faculty of Civil and Environmental Engineering, Gdansk University of Technology, Narutowicza 11/12, Gdańsk 80-233, Poland. (adams@pg.gda.pl)